

# Numerical analysis of the mechanical response of wood glulam beams reinforced through the thickness by FRP rods.

Giuseppe Giambanco<sup>1</sup>, Tiziana Turetta<sup>1</sup>, Alessia Cottone<sup>1</sup>

<sup>1</sup>*Department of Structural, Aerospace and Geotechnical Engineering, University of Palermo, Italy*  
*E-mails: ggiamb@unipa.it, turetta@unipa.it, alessiacottone@unipa.it*

*Keywords:* wood glulam beam, through-thickness reinforcement, interface.

**SUMMARY.** The modern use of through-thickness reinforcement in wood glulam (glued laminated) beams, bridging the potential delamination crack faces, has shown to be an effective technological solution to improve their interlaminar fracture strength. In this paper, the behaviour of wood glulam beams is investigated from an experimental and numerical point of view, comparing the mechanical response of unreinforced and reinforced (by FRP rods) beams subjected to four points bending tests. For the numerical analysis, a simple two-phases (joint and reinforcement) interface model has been formulated and implemented in a finite element code. In particular, the classical interface model for adhesive joint, able to describe the debonding between adjacent laminae, has been enriched to take into account the heterogeneity due to the transversal reinforcement.

## 1 INTRODUCTION

Glulam beams, obtained bonding wood laminae of limited width and length, in order to create structural elements with huge flexibility and reduced wood imperfections, present an intrinsic composite nature: constituents may have different qualities and their assembly occurs through longitudinal adhesive joints. Moreover, since often each lamina does not have a length able to cover the longitudinal development of the beam, a finger joint between two adjacent laminae is necessary.

The global mechanical behaviour of these beams depends on the mechanical properties of each lamina and the adhesive joints. To enhance the mechanical properties of these wood beams, both in terms of strength and stiffness, several prototypes have been realized in form of FRP laminae externally bonded to the beam or internally embedded during manufacturing process [1], [2]. A further reinforcement technique, which is the object of the study, based on the one recently used for composite laminates, consists in the introduction of FRP rods through the beam thickness direction. This transversal reinforcement increases the delamination toughness both in mode I and II as experimental tests, performed on through-thickness reinforced composite laminates, show.

The reinforcement rod in pure mode I opposes to the crack opening displacement through a bridging axial force initially proportional to the relative displacement up to the pull-out of the rod from the composite matrix. Shear tests (pure mode II) demonstrate that the single pin reacts to the relative tangential displacement by shear forces and bending moments, which are elastically related to the displacement jump as long as a multiplicity of failure resin micro-mechanisms appear.

A classical interface model able to catch the main kinematical phenomena that characterize the delamination can describe effectively the non-linear delamination process between adjacent laminae whereas an enriched interface model has to be defined to take into account the heterogeneity due to the presence of through-thickness reinforcement.

Therefore, the principal aim of the paper is to develop a constitutive framework able to describe the anisotropic elastic and post-elastic interface response caused by the through-thickness heterogeneity. In particular a simple and original two-phases (joint and reinforcement) interface model is

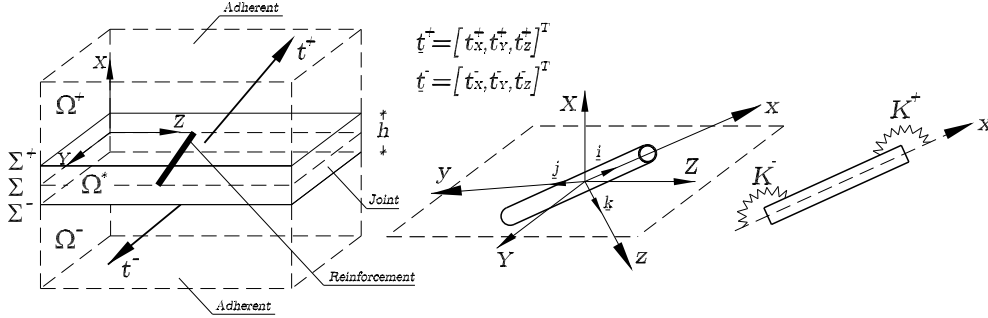


Figure 1: Interface model: general assumptions.

formulated: the two phases, having two independent constitutive laws, are coupled at the equilibrium level. The relevant advantage is to conjugate in a simple way two or more phases, even with different constitutive behaviours. The mechanical behaviour of unreinforced and reinforced (by FRP rods) wood glulam beams is investigated subjecting the beams to experimental and numerical four points bending tests. The numerical analysis has been carried out by a finite element code (FEAP) in which the two-phase interface constitutive laws have been implemented.

## 2 BASIC ASSUMPTIONS AND ELASTIC RESPONSE

The interface model for heterogeneous joints, reinforced by short rods, is developed following a similar approach to that used by the authors in [3]. Two different phases are distinguished: the adhesive joint and the reinforcement, the latter considered as a beam element.

The static and kinematics quantities of the interface are referred to a Cartesian coordinate system  $(X, Y, Z)$  with  $Y, Z$  axes lying within the middle plane  $\Sigma$  of the joint  $\Omega^*$  and the  $X$  axis directed towards the body  $\Omega^+$ , fig. 1a.

The strain state of the joint is assumed constant along the thickness  $h$  and classically described as function of displacement discontinuities at the interface:

$$\boldsymbol{\varepsilon}_J = [\varepsilon_{JX} \quad \gamma_{JY} \quad \gamma_{JZ}]^T = \frac{(\mathbf{U}^+ - \mathbf{U}^-)}{h} = \frac{[\mathbf{U}]}{h}, \quad (1)$$

where  $\mathbf{U}^\pm = [U_X^\pm \quad U_Y^\pm \quad U_Z^\pm]^T$  are the displacement vectors at the interfaces  $\Sigma^\pm$  and  $[\mathbf{U}]$  the displacement discontinuity vector.

The traction components  $\mathbf{t}^+$  on  $\Sigma^+$  and  $\mathbf{t}^-$  on  $\Sigma^-$  can be regarded as external surface loads for the joint  $\Omega^*$ . The stress state of the adhesive phase  $\boldsymbol{\sigma}_J = [\sigma_J \quad \tau_{JY} \quad \tau_{JZ}]^T$  is related to the elastic strain by the linear constitutive law in the following form:

$$\boldsymbol{\sigma}_J = \mathbf{E}_J \boldsymbol{\varepsilon}_J^e, \quad (2)$$

being  $\mathbf{E}_J = [E_{JN} \quad E_{JT} \quad E_{JT}]$  the elastic joint stiffness matrix,  $E_{JN}$  and  $E_{JT}$  the normal and tangential elastic moduli of the joint material.

The joint is reinforced through the thickness by a number  $n_F$  of cylindrical fibres, all oriented in

the same direction. Each fibre is referred to the coordinate system  $x, y, z$  with  $x$ -axis coinciding with the fibre axis, fig.1b and is considered as a Timoshenko beam of length  $l_R$  semi-clamped at the extremities by rotational springs of stiffness  $K^+$  and  $K^-$ , except for the twisting rotation which is free. The circular cross section is characterized by an area  $A_R$ , bending moment of inertia  $I$  and shear factor  $\chi$ .

The kinematics of the beam is described by the continuous displacements  $\mathbf{u}(x)$  and strain fields  $\mathbf{q}(x)$  defined as:

$$\mathbf{u}(x) = [\mathbf{u}_u \mid \mathbf{u}_\varphi]^T = [u_x \ u_y \ u_z \mid \varphi_y \ \varphi_z]^T, \quad (3)$$

$$\mathbf{q}(x) = [e_x \ e_y \ e_z \ k_y \ k_z]^T. \quad (4)$$

In the following, for simplicity's sake,  $\mathbf{u}(\frac{l_R}{2}) = \mathbf{u}^+$ ,  $\mathbf{u}(-\frac{l_R}{2}) = \mathbf{u}^-$  is assumed.

Under the previous hypotheses, the compatibility equations together with the boundary conditions read:

$$\mathbf{q}(x) = \tilde{\mathbf{B}}(x) (\mathbf{u}^+ - \mathbf{u}^-) = \tilde{\mathbf{B}}(x) [\mathbf{u}], \quad -\frac{l_R}{2} < x < \frac{l_R}{2} \quad (5)$$

$$\mathbf{u}_\varphi^+ = \mathbf{A}^+[\mathbf{u}], \quad \mathbf{u}_\varphi^- = \mathbf{A}^-[\mathbf{u}], \quad \mathbf{u}_u\left(\frac{l_R}{2}\right) = \mathbf{u}_{\mathbf{u}^+}, \quad \mathbf{u}_u\left(-\frac{l_R}{2}\right) = \mathbf{u}_{\mathbf{u}^-} \quad (6)$$

being  $\tilde{\mathbf{B}}(x)$  the compatibility matrix defining the continuous strain field as function of the displacement discontinuity  $[\mathbf{u}]$ :

$$\tilde{\mathbf{B}}(x) = \begin{bmatrix} \tilde{\mathbf{B}}_1 \\ \tilde{\mathbf{B}}_2(x) \end{bmatrix} = \begin{bmatrix} 1/l_R & 0 & 0 \\ 0 & S_y & 0 \\ 0 & 0 & S_z \\ 0 & 0 & C_y(x) \\ 0 & C_z(x) & 0 \end{bmatrix} \quad (7)$$

with

$$S_{z,y} = -\frac{12\chi E_R I [E_R I (K^+ + K^-) \mp l_R K^+ K^-]}{l_R d_{y,z}}, \quad (8)$$

$$d_{z,y} = G_R A_R l_R^3 K^+ K^- + 12E_R^2 I^2 [G_R A_R l_R \pm \chi (K^+ + K^-)] + 4E_R I l_R [3\chi K^+ K^- \pm G_R A_R l_R (K^+ + K^-)], \quad (9)$$

and

$$C_{z,y}(x) = \pm \frac{6G_R A_R \{2l_R K^+ K^- x + E_R I [l_R (K^+ - K^-) + 2(K^+ \pm K^-) x]\}}{l_R d_{z,y}}, \quad (10)$$

$$\mathbf{A}^\pm = \begin{bmatrix} 0 & 0 & A_y^\pm \\ 0 & A_z^\pm & 0 \end{bmatrix}, \quad (11)$$

$$A_y^\pm = -\frac{6E_RIG_R A_R(2E_R I + l_R K^\pm)}{d_y}, \quad A_z^\pm = \frac{6E_RIG_R A_R(2E_R I - l_R K^\pm)}{d_z}. \quad (12)$$

In absence of any distributed generalized forces along the beam length, the internal forces

$$\mathbf{Q}(x) = [\mathbf{Q}_u \mid \mathbf{Q}_\varphi]^T = [N \ T_y \ T_z \mid M_y \ M_z]^T \quad (13)$$

arise due to the displacement imposed at the fibre extremities. The axial ( $N$ ) and shear internal forces ( $T_y$  and  $T_z$ ) are therefore constant along the beam, whereas the bending moments ( $M_y$  and  $M_z$ ) vary linearly. The equilibrium equation with its boundary conditions can be written as:

$$\mathbf{Q}'(x) - \mathbf{B}^T \mathbf{Q}(x) = \mathbf{0}, \quad -\frac{l_R}{2} < x < \frac{l_R}{2} \quad (14)$$

$$\mathbf{v}_\varphi^+ = \mathbf{K}^+ \mathbf{u}_\varphi^+, \quad \mathbf{v}_\varphi^- = \mathbf{K}^- \mathbf{u}_\varphi^-, \quad \mathbf{v}_u^+ = \mathbf{Q}_u^+, \quad \mathbf{v}_u^- = -\mathbf{Q}_u^-. \quad (15)$$

The components of the matrix  $\mathbf{K}^-$  and  $\mathbf{K}^+$  are the rotational springs stiffness at the extremities of the beam:

$$\mathbf{K}^+ = [-K^+ \ K^+], \quad \mathbf{K}^- = [K^- \ -K^-] \quad (16)$$

The elastic response of the beam is described by the classical constitutive law:

$$\mathbf{Q}(x) = \mathbf{\Phi} \mathbf{q}(x), \quad -\frac{l_R}{2} < x < \frac{l_R}{2}, \quad (17)$$

where

$$\mathbf{\Phi} = [\mathbf{\Phi}_1 \mid \mathbf{\Phi}_2] = \left[ E_R A_R \quad \frac{G_R A_R}{\chi} \quad \frac{G_R A_R}{\chi} \mid E_R I \quad E_R I \right] \quad (18)$$

is the elastic stiffness matrix, in which  $E_R$  and  $G_R$  are the elastic normal and tangential moduli of the beam.

### 2.1 Elastic response of the heterogeneous joint

Considering the periodic arrangement of figure 2, the joint can be subdivided into  $n_F$  small cells, each one containing only one single reinforcement fibre. With reference to the representative volume element (RVE), having domain  $V_r$  and upper/lower surface boundary  $A_r^\pm$ , the linear elastic behaviour of the reinforced joint permits to establish the existence of the total potential energy  $\Pi$ :

$$\begin{aligned} \Pi = \Pi_J + \Pi_F = & \frac{1}{2} \int_V \boldsymbol{\sigma}_J^T \boldsymbol{\varepsilon}_J dV - \int_{A_r^+} \mathbf{t}^{+T} \mathbf{U}^+ dA - \int_{A_r^-} \mathbf{t}^{-T} \mathbf{U}^- dA \\ & + \frac{1}{2} \int_{-l_R/2}^{l_R/2} \mathbf{Q}^T \mathbf{q} dx - \mathbf{v}_u^{+T} \mathbf{u}_u^+ - \mathbf{v}_u^{-T} \mathbf{u}_u^- - \frac{1}{2} \mathbf{v}_\varphi^{+T} \mathbf{u}_\varphi^+ - \frac{1}{2} \mathbf{v}_\varphi^{-T} \mathbf{u}_\varphi^-. \end{aligned} \quad (19)$$

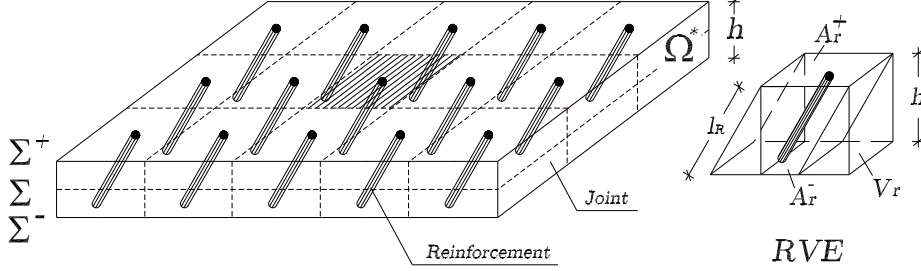


Figure 2: Fibre reinforced interface: periodic cells and representative volume element.

Introducing eqs (2), (6), (15) and (17) and using the transformation  $\mathbf{u} = \mathbf{T}\mathbf{U}$ ,  $\Pi$  can be written as function of the reinforced interface degrees of freedom  $\mathbf{U}^+$  and  $\mathbf{U}^-$ :

$$\begin{aligned}
\Pi(\mathbf{U}^+, \mathbf{U}^-) = & \frac{1}{2} \int_{A_r} \left( [\mathbf{U}]^T \frac{\mathbf{E}_J}{h} \mathbf{U}^+ - [\mathbf{U}]^T \frac{\mathbf{E}_J}{h} \mathbf{U}^- - 2\mathbf{t}^{+T} \mathbf{U}^+ - 2\mathbf{t}^{-T} \mathbf{U}^- \right) dA + \\
& + \frac{1}{2A_r} \int_{A_r} \int_{-l_R/2}^{l_R/2} [\mathbf{U}]^T \mathbf{T}^T \tilde{\mathbf{B}}^T(x) \Phi \tilde{\mathbf{B}}(x) \mathbf{T} [\mathbf{U}] dx dA + \\
& - \frac{1}{A_r} \int_{A_r} \left( \mathbf{v}_u^{+T} \mathbf{T} \mathbf{U}^+ + \mathbf{v}_u^{-T} \mathbf{T} \mathbf{U}^- \right) dA + \\
& - \frac{1}{2A_r} \int_{A_r} \left( [\mathbf{U}]^T \mathbf{T}^T \mathbf{A}^{+T} \mathbf{K}^+ \mathbf{A}^+ \mathbf{T} [\mathbf{U}] + [\mathbf{U}]^T \mathbf{T}^T \mathbf{A}^{-T} \mathbf{K}^- \mathbf{A}^- \mathbf{T} [\mathbf{U}] \right) dA.
\end{aligned} \tag{20}$$

In (20)  $A_r^+ = A_r^- = A_r$  and  $V_r = hA_r$  is assumed.

The equilibrium equations are derived by the minimum condition of the total potential energy:

$$\delta \Pi = \frac{\partial \Pi}{\partial \mathbf{U}^-} \delta \mathbf{U}^- + \frac{\partial \Pi}{\partial \mathbf{U}^+} \delta \mathbf{U}^+ = 0 \quad \forall \delta \mathbf{U}^-, \delta \mathbf{U}^+ \neq 0. \tag{21}$$

From equation (21) making use of the positions:

$$\mathbf{t} = \frac{\mathbf{t}^+ - \mathbf{t}^-}{2}, \quad \mathbf{V}_u = \frac{\mathbf{V}_u^+ - \mathbf{V}_u^-}{2} = \frac{\mathbf{T}^T \mathbf{v}_u^+ - \mathbf{T}^T \mathbf{v}_u^-}{2}, \tag{22}$$

$$\hat{\mathbf{V}}_u = \hat{\mathbf{V}}_u^+ + \hat{\mathbf{V}}_u^- = \mathbf{T}^T \mathbf{A}^{+T} \mathbf{v}_\varphi^+ + \mathbf{T}^T \mathbf{A}^{-T} \mathbf{v}_\varphi^-, \tag{23}$$

the following equilibrium equation for the reinforced joint is derived:

$$\mathbf{t} + \frac{\mathbf{V}_u}{A_r} + \frac{\hat{\mathbf{V}}_u}{A_r} = \boldsymbol{\sigma}_J + \boldsymbol{\sigma}_F. \tag{24}$$

The resultant of the additional contact layer tractions  $\sigma_F$ , related to the reinforcement presence and constant on the cell middle surface  $A_r$ , produces the same virtual work as the one produced by the internal forces along whole fibre length.

$$\sigma_F = \frac{1}{A_r} \int_{-l_R/2}^{l_R/2} \mathbf{T}^T \tilde{\mathbf{B}}^T(x) \Phi \tilde{\mathbf{B}}(x) [\mathbf{u}] dx. \quad (25)$$

Furthermore, using the compatibility matrix partition (7),  $\sigma_F$  can be splitted into two different contributes:  $\sigma_{F1}$  is associated to normal and shear fibre internal forces,  $\sigma_{F2}$  to the bending moments.

$$\sigma_{F1} = \frac{l_R}{A_r} \mathbf{T}^T \tilde{\mathbf{B}}_1^T \Phi_1 \tilde{\mathbf{B}}_1 [\mathbf{u}], \quad (26a)$$

$$\sigma_{F2} = \frac{1}{A_r} \int_{-l_R/2}^{l_R/2} \mathbf{T}^T \tilde{\mathbf{B}}_2^T(x) \Phi_2 \tilde{\mathbf{B}}_2(x) [\mathbf{u}] dx. \quad (26b)$$

Resolving the r.h.s. of equations (26) it is also easy to verify that:

$$\frac{\mathbf{V}_u}{A_r} = \sigma_{F1}, \quad \hat{\mathbf{V}}_u = \sigma_{F2}. \quad (27)$$

Equation (26b) shows that the bending contribute along the whole fibre length is smeared on the middle interface surface by two shearing forces. From eqs (25), (1) and (2) the stiffness of the reinforced joint can be obtained:

$$\mathbf{K}_{JR} = \mathbf{K}_J + \mathbf{K}_R = \frac{\mathbf{E}_J}{h} + \frac{1}{A_r} \int_{-l_R/2}^{l_R/2} \mathbf{T}^T \tilde{\mathbf{B}}^T(x) \Phi \tilde{\mathbf{B}}(x) \mathbf{T} dx. \quad (28)$$

### 3 POST-ELASTIC RESPONSE OF THE HETEROGENEOUS JOINT

The interface constitutive laws, relating the contact tractions  $\mathbf{t}$  with the displacement discontinuities  $[\mathbf{U}]$ , are defined by the constitutive equations of each single phase namely the thin adhesive layer and the reinforcement fibre.

#### 3.1 Joint response

The constitutive behaviour adopted for the adhesive phase is derived in a thermodynamically consistent approach in the context of damage mechanics: the main constitutive equations are reported in [3].

#### 3.2 Reinforcement response

The post-elastic response of the reinforcement rod is described in detail in the paper of Cox and Shridar [4]. Following their problem schematization, a uniform cross sectional shape rod lies in the X-Z plane and bridges a delamination crack on the plane  $X = 0$ . The bridging rod is inclined relative to the joint delamination plane by the initial angle  $\alpha$ . If deformed, the rod axis deflects through some angle  $\varphi_y(x)$  and  $\varphi_{y0} = \varphi_y(0)$  is the deflection angle in correspondence to the fracture surface. Following the terminology introduced in [4], the angle  $\varphi_{y0}$  may have the same or different sign as the initial slope  $\alpha$ , distinguishing the *against the nap* and *with the nap* loading conditions,

respectively.

The experimental tests show that the failure modes for the rods are substantially different for the two above mentioned loading conditions. For the case of the rod loaded with the nap the axial stress is positive (tension) and in presence of unidirectional composite rod the stiffness of the joint is strongly influenced by the high value of the axial rod stiffness. Two dominant failure mechanisms can occur, namely the *pullout of the rod*, due to the progressive debonding of the reinforcement from the surrounding laminate matrix and the *reinforcement rupture*, reached when the axial stress equals the tensile strength of the rod.

If the bridging rod is loaded against the nap, the axial stress is initially negative (compression) and the tendency of the rod to shear and deflect is maximized. The bending and shear stiffness of the rod influence the joint response and for composite rods, because of relevant shear stresses, numerous *matrix cracks*, parallel to the rod direction, appear up to the complete separation of fibres from the matrix. In this case the rod becomes a set of independent strands and it can accommodate large rotations orienting along the load direction, therefore the composite reinforcement loses shear and bending stiffness and turns into a truss element, i.e. reacting only to axial forces. Also in this case the ultimate failure can occur by two mechanisms: the rupture under tension or, in the case of short rod, the pullout from the laminate.

The goal of the present paper is to describe each failure mechanisms above illustrated, making use of a non-linear constitutive law for the rod phase based on the classical concepts of solid mechanics like as plasticity and continuous damage theories.

The *pullout failure mechanism* occurs if the composite rod is subjected to tensile axial force ( $N_F > 0$ ). At the beginning the rod reacts elastically mainly by its axial stiffness up to the pullout (due to the progressive debonding from the laminate matrix) takes place. The pullout is here simulated by an elasto-plastic model for which anelastic discontinuous displacements evolve if a limit elastic axial force is reached. The evolution of slipping discontinuous displacements is governed by a simple bilinear  $N_F - [u_x]$  constitutive law in which the limit elastic and final (corresponding to the pullout of the rod) discontinuous displacements are  $[u_x]_0$  and  $[u_x]_f$ :

$$N_F = H_{uf} \frac{E_R A_R}{l_R} ([u_x] - [u_x^s]), \quad (29)$$

where  $H_{uf}$  is a Heaviside function defined as  $H_{uf} = H([u_x]_f - [u_x])$  in which  $H(\bullet) = 0$  if  $(\bullet) < 0$ ,  $H(\bullet) = 1$  if  $(\bullet) > 0$ .

The failure mechanism is activated if the following yield pullout condition is verified

$$\Phi_s(N_F, \chi_p) = N_F - N_0 - \chi_p = 0. \quad (30)$$

The additive decomposition of the axial strain in the elastic and plastic parts is postulated:

$$e_x = e_x^e + e_x^s = \frac{1}{l_R} ([u_x^e] - [u_x^s]). \quad (31)$$

The evolution of slipping discontinuous displacement is described by the following associative plastic flow rules and loading-unloading conditions

$$[\dot{u}_x^s] = \dot{\lambda}, \quad \dot{\xi}_p = \dot{\lambda}; \quad \Phi_s \leq 0, \quad \dot{\lambda} \geq 0, \quad \dot{\lambda} \Phi_s = 0 \quad (32)$$

where  $\dot{\lambda}$  is the plastic multiplier,  $N_0 = [u_x]_0 E_R A_R / l_R$  represents the pull-out activation threshold and  $\chi_p$  is the static internal variable defined as  $\chi_p = h_p \xi_p$ , being  $h_p$  the hardening parameter. In

particular,  $h_p = 0$  can be chosen for long rods and  $h_p < 0$  for short ones.

The *reinforcement rupture* under tensile axial forces is described making use of classical concepts of Damage Mechanics. The progressive stiffness degradation of the rod is analytically described by:

$$N_F = H_{uf} (1 - \omega_s)^2 \frac{E_R A_R}{l_R} [u_x^e]. \quad (33)$$

The damage variable  $\omega_s$  assumes values in the range  $0 \leq \omega_s \leq 1$ . The damage activation function is assumed with the following form:

$$\Phi_d(\zeta_d, \chi_d) = \zeta_d - \zeta_0 - \chi_d \leq 0 \quad (34)$$

where  $\zeta_d$  is the thermodynamic force conjugated to  $\omega_s$  and  $\chi_d$  is the static variable conjugated to the internal variable  $\xi_d$ :

$$\zeta_d = (1 - \omega_s) \frac{E_R A_R}{l_R} [u_x^e]^2, \quad \chi_d = h_d \xi_d. \quad (35)$$

The flow rules and the loading/unloading conditions read respectively:

$$\dot{\omega}_s = \dot{\lambda}_d, \quad \dot{\xi}_d = \dot{\lambda}_d; \quad \Phi_d \leq 0, \quad \dot{\lambda}_d \geq 0, \quad \dot{\lambda}_d \Phi_d = 0. \quad (36)$$

In order to describe the *beam-truss degeneration*, Damage Mechanics has been applied to the bending and shear stiffness of the rod. The kinematic variables driving this failure mechanism are the rotation angles at the two extremities  $\varphi_y^\pm = \varphi_y(\pm \frac{l_R}{2})$ , depending on the shear and bending stiffness of the rod and on the rotational springs stiffness  $K$  ( $K^+ = K^- = K$  is assumed for sake of simplicity):

$$\varphi_y^\pm = \varphi_y = - \frac{6E_R I G_R A_R [u_z]}{G_R A_R l_R^2 K + 6E_R I (G_R A_R l_R + 2\chi K)}. \quad (37)$$

An integrity function is applied to the stiffness of the rotational springs, therefore, in equation (37) the stiffness value  $K$  is replaced by

$$\tilde{K} = (1 - \omega_c) K \left( \frac{[u_x^s] - [u_x]_f}{-[u_x]_f} \right)^2 \quad (38)$$

in which  $\omega_c$  is the damage variable assuming the zero value for a sound rod matrix and the unit value when the rod matrix is totally damaged and the fibres become a set of strands, i.e. truss mechanical behaviour.  $\omega_c$  is defined as function of the damage history variable  $\varphi_{yd}$  as follows:

$$\omega_c = \frac{\varphi_{yd}^2}{\varphi_{yd}^2 + h_c} \quad (39)$$

where  $h_c$  is a constitutive parameter. The matrix damage onset is regulated by the following damage function with the loading-unloading conditions:

$$\Phi_{dc} = \varphi_y - \varphi_{yd} - \varphi_{y0} \leq 0; \quad \Phi_{dc} \leq 0, \quad \dot{\varphi}_{yd} \geq 0, \quad \dot{\varphi}_{yd} \Phi_{dc} = 0. \quad (40)$$

In equation (40)  $\varphi_{y0}$  represents the damage activation threshold.

The reinforcement reduced to a set of strands, can suffer large rotations determined by the applied total discontinuity displacement following the direction of the applied loading condition. The rupture of strands under tension characterizes the final failure mechanism.

#### 4 APPLICATIONS TO WOOD STRUCTURES: GLULAM BEAMS

Four points bending tests on real-scale wood glulam beams have been carried out at the DISAG Laboratory of Palermo University. The glulam beam T3-1 is constituted by 12 laminae, 4 of wood denoted L30 ( $\sigma_k=18$  MPa,  $E=12$  GPa) and 8 (beam core) of wood L25 ( $\sigma_k=14.5$  MPa,  $E=11$  GPa). The experimental tests regarded a simple glulam beam and a glulam beam reinforced with GFRP rods inserted in the normal direction to the laminae. In both cases the beams have been subjected to force-controlled tests.

The numerical analysis of the unreinforced glulam beam has been carried out by the research oriented finite element code (FEAP) in which the through-thickness interface laws have been implemented. Space discretization has been achieved employing two-dimensional 4 nodes isoparametric elements simulating laminae and by 4 nodes interface elements for the bed and finger joints, for a total of 1980 nodes and 1862 elements. The comparison between unreinforced experimental load-

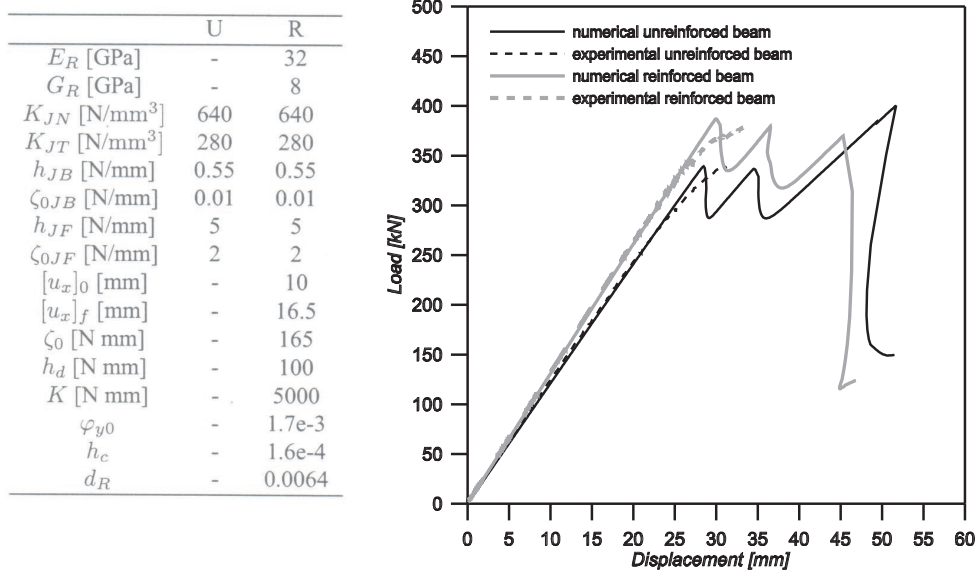


Figure 3: Comparison between experimental and numerical unreinforced and reinforced glulam beam load-displacement curves and constitutive parameters used for the numerical analysis (U=unreinforced, R=reinforced) (JB=bed joint, JF= finger joint).

displacement curve and the numerical one is shown in fig. 3. The numerical results match quite well the experimental ones both in terms of elastic response and peak load value attained during the test. After an initial elastic response, non linear effects occur due to the delamination along the longitudinal joints. Once the peak load has been reached a softening branch with unstable response takes place due to a collapse mechanism corresponding to the progressive slipping of the bed joints which has been also observed experimentally up to the final greatest slip reached at the middle plane. The constitutive parameters adopted for the numerical simulation are reported in table of figure 3.

The second test has regarded another glulam beam T3-1 RV (with a different geometrical distribution of finger joints) reinforced by 64 GFRP rods having a diameter  $\phi = 8$  mm and a length  $l = 370$  mm embedded in the beam through an epoxy-amino resin. The rods have been distributed in two rows between the load application points and the supports in order to improve the delamination

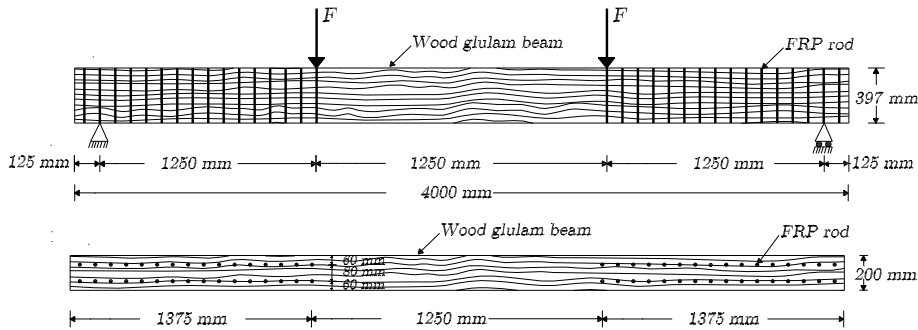


Figure 4: Geometrical scheme of the rods location in the glulam beam T3-1 RV.

toughness and to increase the overall beam strength. In figure 4 the geometrical scheme of the rods location is reported. As done for the previous test, the glulam beam has been subjected to a four points bending test and the vertical forces have been increased up to beam failure. The comparison between reinforced experimental and numerical results, in terms of load-displacement curves, is reported in figure 3. It can be noticed that the reinforced glulam beam shows an increment of stiffness and the peak load attained is 380 kN, that is 10% higher than the unreinforced value detected (350 kN). The failure mechanism observed both experimentally and numerically is not so much different from the one observed in the unreinforced glulam beam test, thus the peak load increment depends on the modest increase of bed joints toughness. New chances for the future are the comparison of numerical post peak results with experimental ones derived from displacement controlled tests and the employment of different materials for the through-thickness reinforcement.

#### Acknowledgements

The authors acknowledge the financial support given by the Italian Ministry of Education University and Research (MIUR) under the PRIN07 Project 2007YZ3B24, “Multi-scale problems with complex interactions in Structural Engineering”.

#### References

- [1] Davalos, J.F., Qiao, P.Z. and Trimble, B.S., “Fiber-reinforced composite and wood bonded interface, part 1,” *Journal of Composites Technology and Research ASTM*, **22**, 224-231 (2000).
- [2] Tascioglu, C., Goodell, B., Lopez-Anido, R., “Bond durability characterization of preservative treated wood and E-glass/phenolic composite interfaces,” *Composites Science and Technology*, **63**, 979-991 (2003).
- [3] Cottone, A., Turetta, T., Giambanco, G., “Delamination Study of through-thickness reinforced composite laminates via two-phase interface model,” *Composites: Part A*, **38**, 1985-1995 (2007).
- [4] Cox, B.N., Sridhar, N., “A traction law for inclined fibre tows bridging mixed-mode cracks,” *Mech. Advanced Materials and Structures*, **9**, 299-331 (2002).